Measurement of Reliable Indentation Elastic Modulus in Brittle Materials from Berkovich Nano Indentation

by

Yan Chen

A thesis submitted to the Graduate Faculty of
Auburn University
in partial fulfillment of the
requirements for the Degree of
Master of Science

Auburn, Alabama
August 6, 2016

Keywords: nanoindentation, thin film, brittle material,
mechanical testing, materials engineering,

Approved by

Barton Prorok, Chair, Professor of Materials Engineering
Ruel A. Overfelt, Professor of Materials Engineering
Majid Beidaghi, Assistant Professor of Materials Engineering

Abstract

Determining the elastic modulus of brittle materials from unloading segments during standard indentation testing is complicated by surface generations of cracks and other defects form. This work describes a method to reliably extract the elastic modulus of brittle materials from Berkovich indents under the continuous stiffness mode. It involves depositing and indenting a metallic film of known Poisson's ratio onto the ceramic. The Zhou-Prorok model is employed and rearranged to express the experimental data as a function of the ceramic substrate's elastic modulus. This generates a linear portion in the curve which directly relates to the substrate modulus and Poisson's ratio. Measuring the slope of the treated experimental data reveals the substrate's values. This method enables the elastic properties of brittle ceramic to be determined by generating and indenting a film/substrate composite with a metallic film. This enables the elastic behavior of the brittle ceramic to be assessed without the indenter penetrating it. This method can assess properties of an unknown film/substrate.

Table of Contents

List of Tables

List of Figures

Chapter 1 : Motivation and Background

1.1 Motivation

Nanoindentation technique depends on three assumptions: the material response being linear elastic, the mechanical property of the test sample being spatially homogeneous, and the contact area being the projected indenter area.

Those assumptions may not be valid in a few extreme conditions. It was known that some materials with a high modulus and low fracture toughness can develop radial cracks during the indentation process [11]. This crack is contributed by the high stress concentration caused by indentation [11, 13]. A more valid measurement requires the elimination of such stress concentration.

Figure 1.1 illustrates this effect for indenting an aluminum oxide single crystal (0001). Here, the elastic modulus is plotted as a function of displacement into the surface, which begins at a high value and then reduces continually as the indenter penetrates. The highest of the value is higher than 1000 GPa and exceeds the possible range of elastic modulus of aluminum oxide and lowest value is at 400 GPa. No consistent value of elastic modulus can be identified. This unsatisfying result illustrates the difficulties of the test on hard brittle materials.

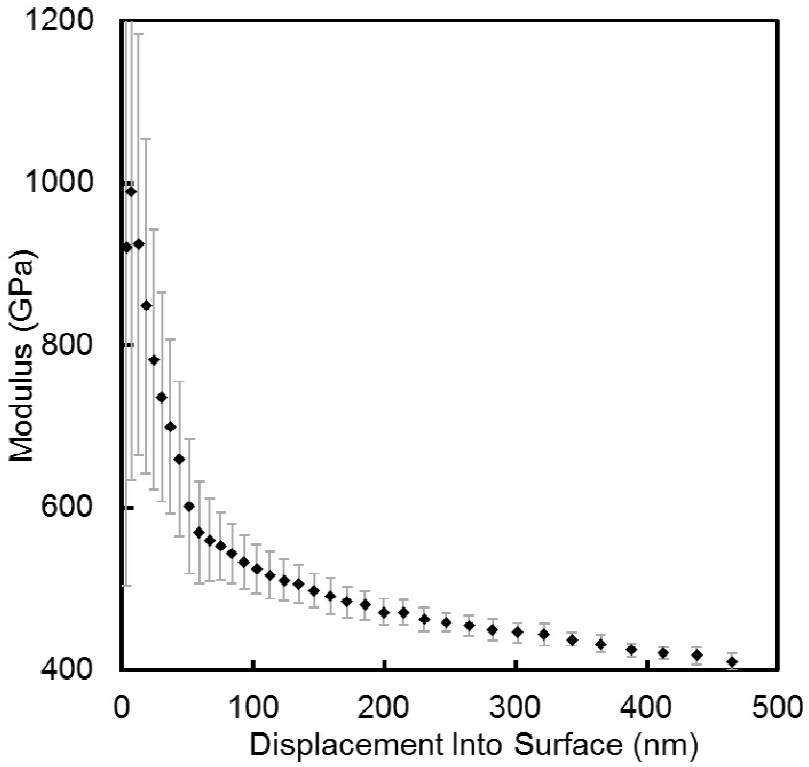

Figure 1.1 Indentation data on Al2O3 single crystal (0001) shows unreliable testing result.

The reasoning behind this phenomenon is the formation of the crack. The indentation of the sample cannot be simply regarded as elastically resembling a smooth rigid indenter contact with an infinite half space with the contact area of the projected indenter area. The contact area cannot simply be calculated by the displacement of the indenter and load stiffness data since the maximum load will be lower than the normal condition. Also, the tested stiffness will not be the same value compared to the stiffness value from the sample without a crack since the stress distribution in the cracked sample was altered.

It will be difficult to directly reduce the effect of cracking on the test results. In this work, another method is developed to provide a new way to solve this problem.

1.2 Oliver and Pharr's Nanoindentation stiffness testing

The development of thin films, coating systems, and the MEMS (microelectronic mechanical systems) requires a reliable way of testing mechanical properties of small samples. Depth sensing indentation, typically nanoindentation, is widely used in those areas [1-7].

Indentation technique has two different origins, one is the hardness testing, which used in many engineering applications, and another is the theory of elastic contact. The ingenuity of the depth sensing indentation technique is the combination of those two which provides a new perspective to both the plastic and elastic properties of materials [5-7].

In this work, a force controlled nanoindentation instrument was used. It consists of an instrument frame to hold both the indenter and the sample, an indenter column which is suspended on supporting springs, a loading coil to exert force directly on the indentation column, a capacitive displacement sensor, and a Bekovich diamond indenter head.

Nanoindentation is essentially a well-recorded, elastic-plastic contact between a near rigid indenter (mostly diamond Berkovich indenter) and the well-polished test-sample. A typical nanoindentation instrument uses a loading coil to precisely control the force exerted onto the sample and a capacitive displacement sensor to record the displacement [5-7].

To test the elastic-plastic properties of materials, the process of indentations is generally divided into three segments: loading segment, where the indenter pushes down into the sample; hold segment, where the indenter holds at constant force while continuing to recording the displacement; unloading segment, the indenter unloads (Figure. 1.1) [5-7]. Displacement data is used to construct the indentation contact area while the maximum loading data is used to calculate the hardness data.

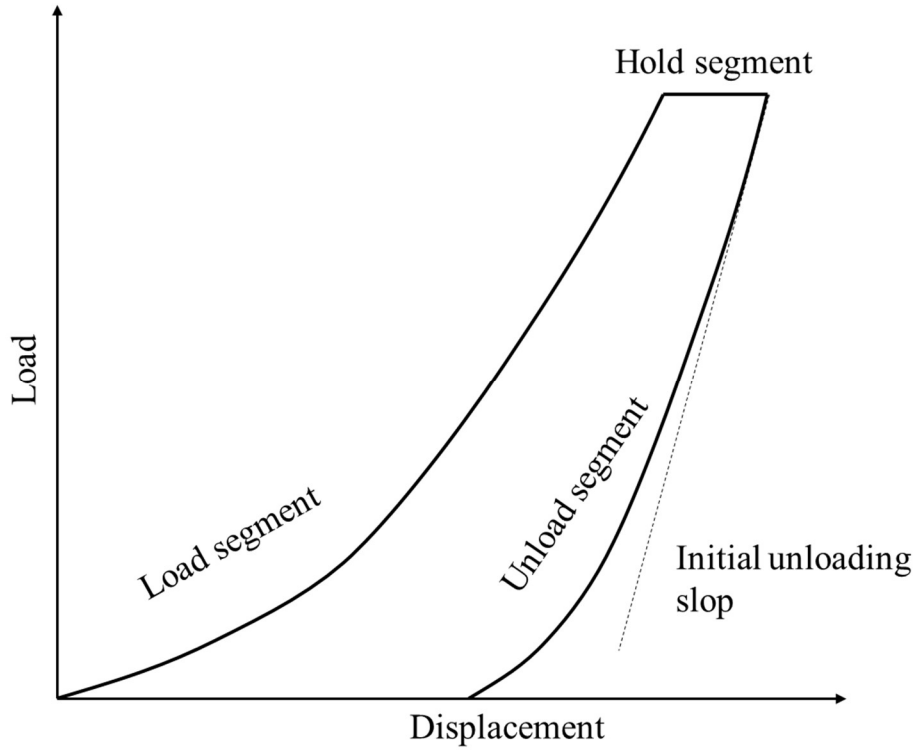

Figure 1.2 Schematic representation of a typical load-displacement curve from nanoindentation

What makes nanoindentation unique is the use of unloading data to construct the elastic modulus of the material. It should be noted that the indentation process involves both plastic and elastic deformation of the specimen. The unloading process of the indentation will only involve the elastic deformation. The reasoning behind that is simple- plastic deformation is irreversible, thus cannot contribute to the spring back.

Oliver and Pharr's method solves three problems in the measuring of elastic properties of materials in instrumented indentation: measurement of the contact area, measurement of the hardness, and measurement of the stiffness [5-7].

The contact area is calculated by the load stiffness curve and calibrated area function by a simple relation:

$$A = F(h_{max} - \epsilon \frac{P_{max}}{S})$$

where ϵ is the geometric constant, and for elastically smooth indenter, $\epsilon = 0.72$ and hardness is calculated by:

$$H = \frac{P_{max}}{A}$$

The property used estimates the elastic modulus based on the measurement of the "initial unloading slop" of the unloading segment. This is called the "stiffness" in the context of the nanoindentation. Oliver and Pharr's method, based on the elastic contact theory originated by Sneddon, uses this relation to estimate the elastic modulus of the material:

$$S = \frac{dP}{dh} = \beta \frac{2}{\sqrt{\pi}} \sqrt{A}\, E_r\,,$$

where S is stiffness, A is the indentation area, and β is a correction factor that related to indenter shape, and the reduced modulus E_r is defined as:

$$\frac{1}{E_r} = \frac{1-\nu^2}{E_t} + \frac{1-\nu_i^2}{E_i}\,,$$

The argument of this relationship is valid to use in indentation unloading [6]. Although the indentation on plastic elastic material is of the shape of Berkovich indenter, the plastic

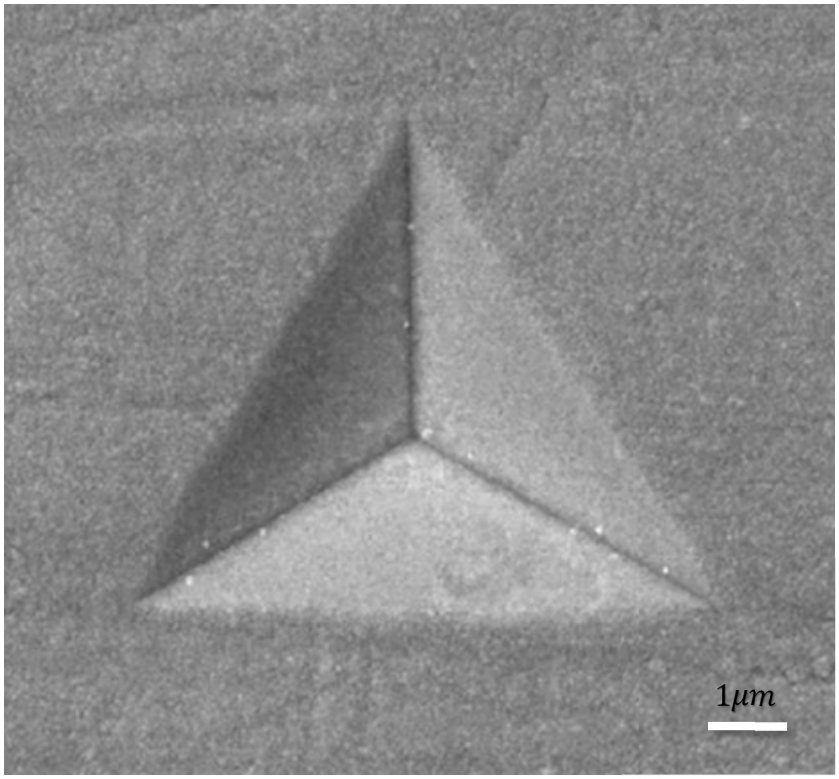

Figure 1.3 A typical residual indents on sample. The length of the scale bar is 1 micron.

deformation will cancel out the strain concentration caused by a sharp tip. This leaves the elastic deformation profile essentially as the one with a smooth indenter and the stiffness modulus relationship works fine with any smooth indenter [6-8].

1.3 Continuous stiffness method (CSM)

A significant improvement in the nanoindentation technique is the CSM (continuous stiffness method). Consider the stiffness measured by the initial unloading slope as a type of static measurement. This stiffness can also be measured dynamically [8].

CSM regards the indenter column as an overdamped, harmonic oscillator under forced vibration. Thus, the test sample worked as a spring with variable stiffness which depended on the loading behavior. From this aspect, the nanoindenter loading column is schematically shown in Figure.1.2. The dynamic behavior of a forced, harmonic oscillator can be described by the differential equation:

$$m\ddot{z} + \lambda\dot{z} + Kz = F_0\sin(\omega t)$$

where m is the effective mass of the indenter, λ is the damping constant, K is the spring constant, and the $F(t)$ is the force. In the context of nanoindentation, mass relates to the mass of the indenter column and the indenter. Damping is contributed by the damping in the position senor, air, and the diamond indenter.

The solution of this differential function is well known [36]:

$$z = z_0 \sin(\omega t + \phi)$$

$$z_0 = \frac{F_0}{k} \frac{1}{\sqrt{(1-r^2)^2 + (2\lambda r)^2}}$$

$$\phi = \arctan(\frac{2\lambda r}{1 + r^2})$$

Above solutions provided a possibility to test stiffness from the dynamic response of the indentation system. The essential idea here is to probe the spring constant of this system at the same frequency. The resonance behavior is suppressed by the high damping in this system.

When the continuous stiffness method is used as the testing process, the indenter column held a constant frequency (below resonance frequency of the system) and a constant vibration amplitude. The only variable in the equation is the applied force. From the applied force, the stiffness of the system can be calculated continuously as a function of the displacement into the surface:

$$\left|\frac{F_0}{z_0}\right| = \sqrt{\left(S_{total} - m\,\omega\right)^2 + \left(\omega\, D\right)^2}$$

where F_0 is the harmonic contact force and z_0 is the oscillation amplitude (harmonic displacement). From the total stiffness, the stiffness of contact is calculated [8].

The instrument used in this work has a simple way to formulate the load which added the harmonic force and the loading force together. The displacement of the vibration and displacement into the surface are provided directly from the instrument. Harmonic displacement is controlled at a constant value when harmonic force is measured.

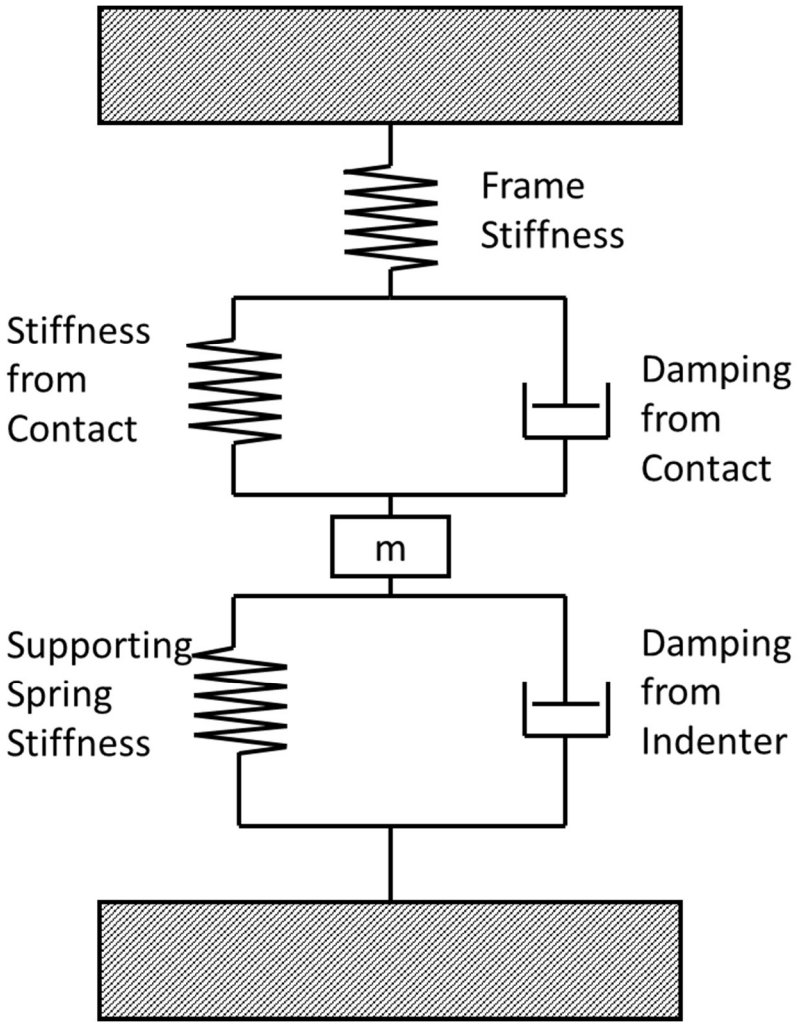

Figure 1.4 The dynamic model schematics of nanoindentation instrument

Chapter 2： Experimental Procedures

2.1 Thin film sputtering and measuring

In this work, two different film-substrate systems were used. Both of them were prepared using Denton Discovery 18 sputtering system. All the samples with same film were sputtered at same time to minimize the possible difference in thickness. A silicon slide with approximately 1 centimeter square was prepared along with samples. Two different films were prepared using the DC sputtering process.

Chromium film was prepared at 200W of sputtering with 860 seconds of sputtering time. Before sputtering, with sputter target shutter closed, the sputter process was performed for 120 seconds. This process is called pre-sputtering. It is used to clean the surface of the target. This process takes a long time for chromium target because chromium target has an oxidation layer that needs to be removed. Gold film was prepared at a lower power of 100W with a pre-sputter time of 60 seconds and a sputtering time of 1715 seconds. Before sputtering the gold film, a thin layer of chromium film (less than 10 nm) was sputtered as an adhesion layer.

After sputtering, the film's thickness was measured by a JEOL JSM 7000F scanning electron microscope (SEM). A cross-section of the film-substrate system was made by the silicon sample. Because its property of fracture along its crystal direction, a clean cross-

section was obtained. Then, the cross-section of film was measured under back scatter mode. Using back scatter imaging eliminates the edge effect that is prominent in second electron mode (figure 2.1).

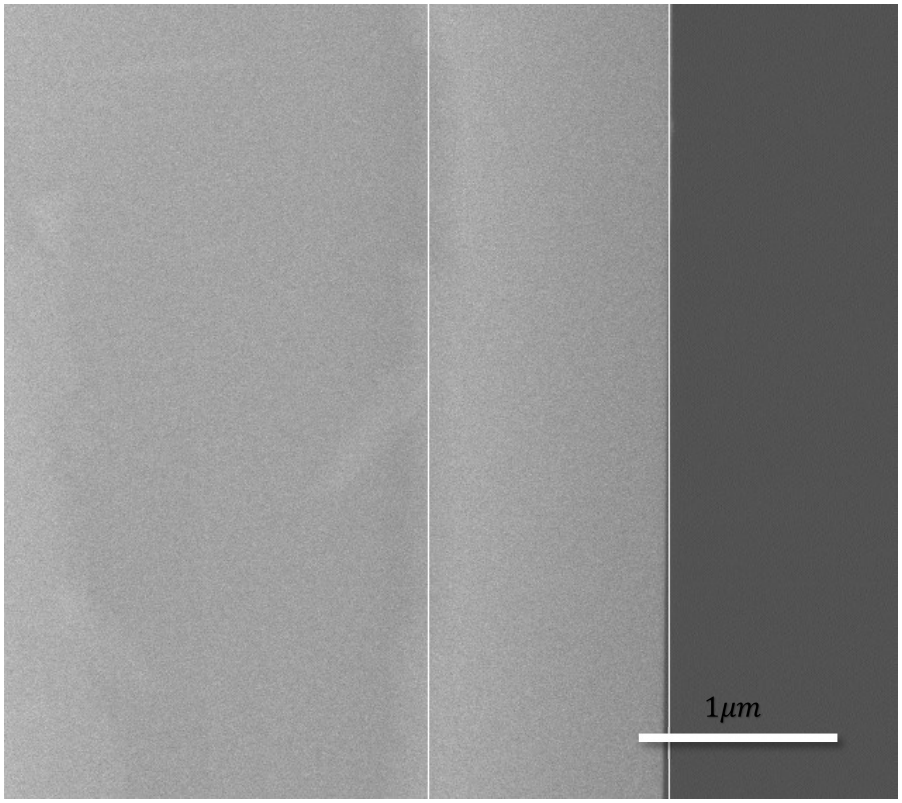

Figure 2.1 Cross-section of Cr film on silica in Back Scatter Image. Two line shows the thickness of film. Scale bar is 1 micron.

2.2 Nanoindentation

Nanoindentation modulus testing in this work is performed on MTS Nanoindenter XP with a Berkovich diamond tip. The testing method used is the XP continuous stiffness method directly from the indenter software. This method directly follows the previously introduced Oliver and Pharr method and Continuous Stiffness Method. This method is also displacement controlled, which means for each test the final displacement of the indenter is controlled by the input displacement goal, not maximum force, which may vary in different tests.

All of the test have the same parameter input except the indentation final displacement. All of the indentation displacement on each group of film-substrate system is the same. For each sample, 25 indents is performed. Indents are in a five-by-five grid with 100 μm of spacing.

Each test is performed using CSM and the testing frequency is set at 45Hz. Target harmonic displacement is set at 2nm. The thermal drift threshold is set at 0.05 nm/s. Before testing, the thermal drift is tested because testing will not perform until the thermal drift test by the indenter is lower than the threshold value.

For each indent, the instrument goes through four different stages. First, the loading segment indenter penetrates the surface of sample at a constant speed. Second, the holding segment indenter holds at a constant load to minimize viscoelasticity's effect on the test. Third, the segment unloads and the stiffness is measured. When unloading is at 90% of the

maximum load, the last segment holds at a constant load. This is used to calculate the thermal drift for each indent.

CSM is activated at each loading segment (data from holding and unloading is discarded). Harmonic displacement is controlled to reach the preset target. Harmonic force is separately detected from the loading force.

After the test, results are averaged using a standard software provided by the indenter instrument. Results of the hardness, elastic modulus, and displacement are calculated using the CSM method and Oliver and Pharr's method.

To view the internal structure of both single crystal ceramic indentation and the film-substrate system, focused ion beam (FIB) experiments were performed on a TESCAN LYRA3 FIB-FESEM system. Results of FIB were imaged by the same system.

2.3 Zhou-Prorok method

Nanoindentation tests performed on a film-substrate system with a film thickness comparable to the indentation displacement will not result in exact film modulus. The result will be mixtures of film and substrate modulus and this phenomenon is called “substrate effect” [14-16]. This is a well understood phenomenon [16-26]. The Zhou-Prorok model was used in this work due to its high accuracy and reliability [25, 26, 34].

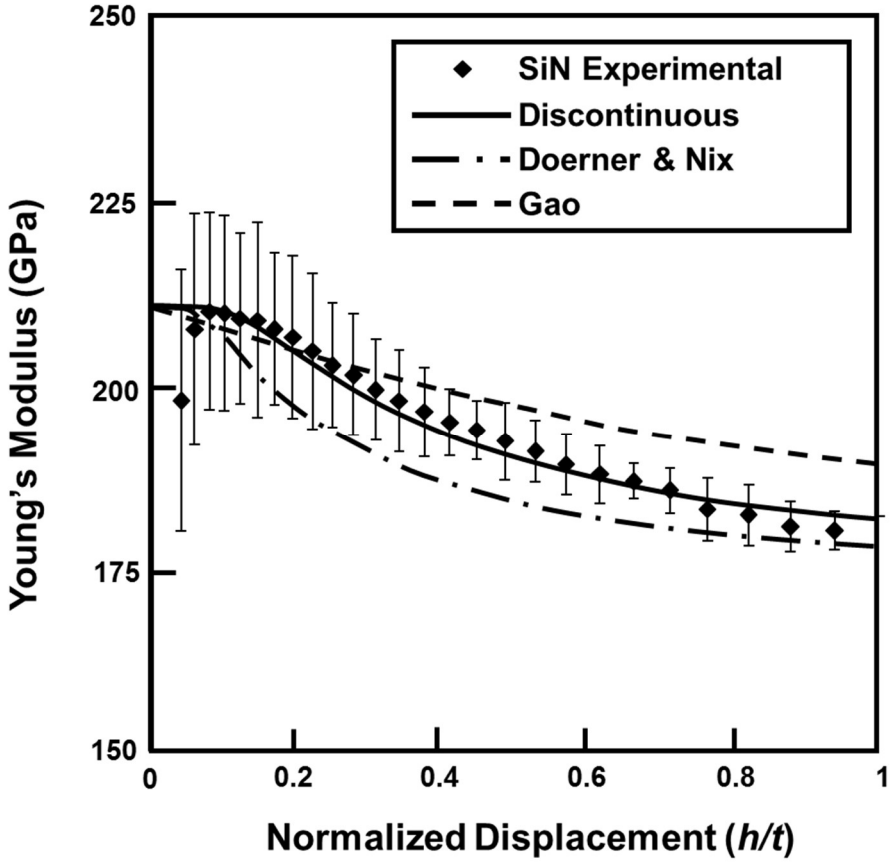

Figure 2.2 Compare Zhou & Prorok model and other two early model with experimental result.

The Zhou-Prorok model is a basic form of the inverse rule of mixtures with weighting factors that describe the interplay between film and substrate, equation 2.1:

$$\frac{1}{E_t} = \frac{1}{E_f}(1 - \Phi_s) \cdot \left(\frac{E_f}{E_s}\right)^{0.1} + \frac{1}{E_s}\Phi_f, \tag{2.1}$$

where E_t is the tested modulus from the indenter, E_f is film modulus, E_s is substrate modulus, the weighting factors $\Phi_f = e^{-\nu_f\left(\frac{t}{h}\right)}$ and $\Phi_s = e^{-\nu_s\left(\frac{t}{h}\right)}$ where υ_f and υ_s are film and substrate Poisson's ratios respectively, t is thickness of the film, and h is displacement into the film. Compared to other models describing the indentation modulus of film-substrate system, this model is quite accurate (figure 2.2).

Chapter 3 : Testing on Brittle materials and Film-Substrate system parameter fitting

3.1 Indentation on brittle materials

Direct indentation of hard, brittle materials is complicated by the formation of cracks and other defects during indenter penetration. These defects hinder assessing the material's elastic modulus which is determined from the elastic unloading of the indent as they reduce the stored elastic energy imparted into the material from the indent loading segment. Consequently, the measured unloading stiffness is lower than expected, resulting in a smaller calculated elastic modulus.

Figure 1.1 shows this effect for indenting an aluminum oxide single crystal (0001). Here no consistent value of elastic modulus can be identified. To illustrate the cause of this result, SEM observation with FIB was used. The load displacement data was analyzed.

The presence of these defects is confirmed in Figures 3.1 and 3.2. Here a discontinuity in the modulus-displacement curve corresponds to a rapid increase in indenter displacement at constant load. This indicates defect generation or initiation of plastic deformation (Figure 3.1). The flat table observed at Figure 3.1 can be explained as induced by nucleation of dislocation inside the crystal. Defects are also seen in scanning electron micrographs (Figure 3.2) along the surface at the indent corners propagate downward into the material. Finding a method of accounting for eliminating the effect of these defects would enable more accurate measurements of their material properties.

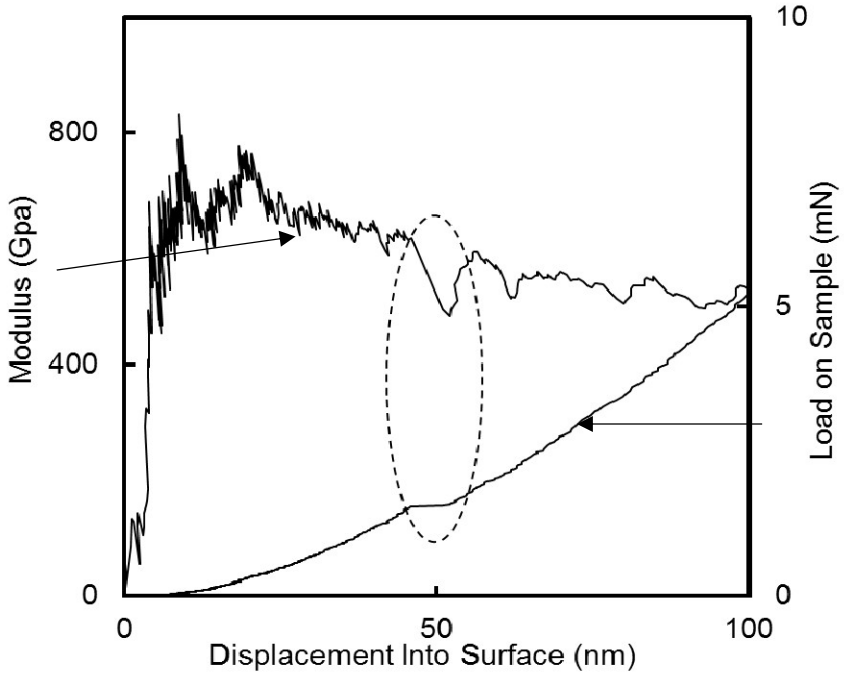

Figure 3.1 Single indentation result shows the disruption on load vs. displacement and its corresponding elastic modulus drop on modulus result.

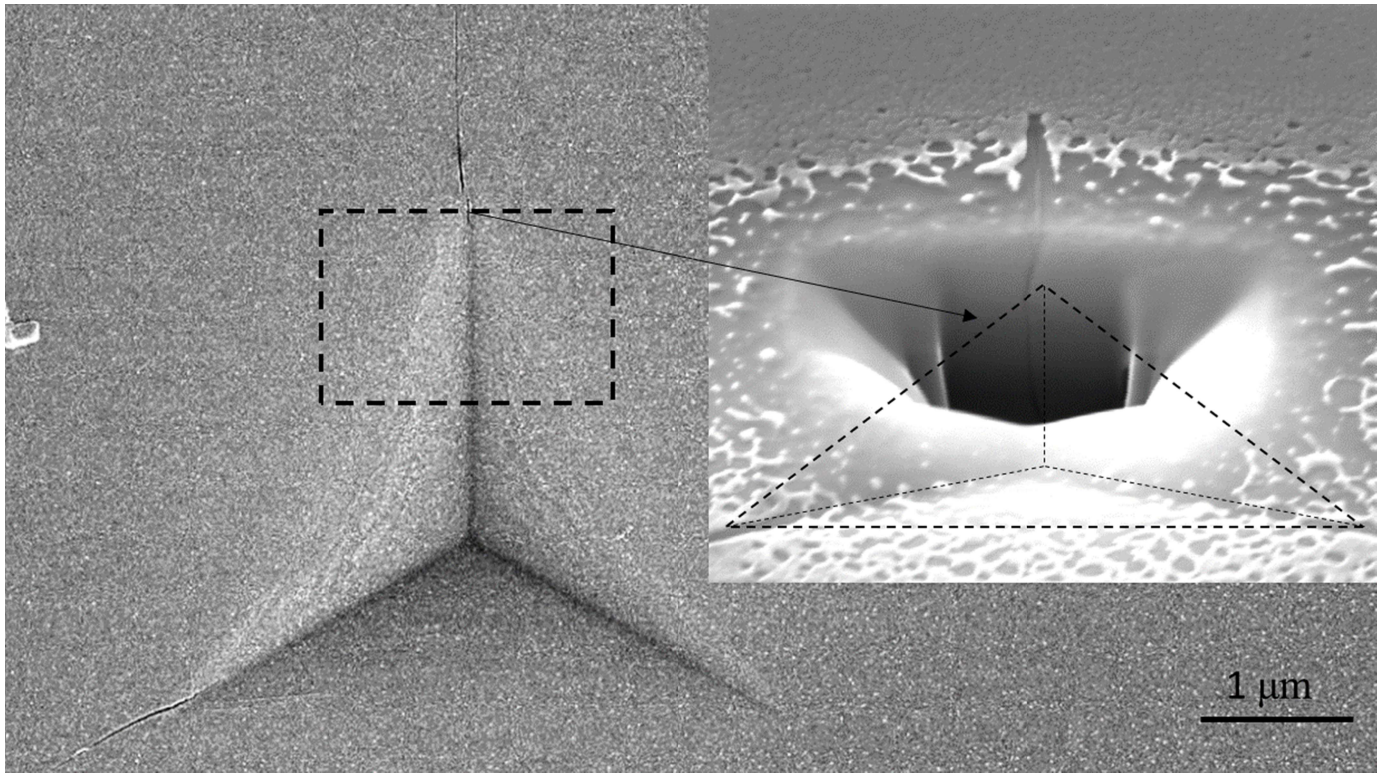

Figure 3.2 Scanning electron microscope of residual indentation on the Al2O3 single crystal (0001). Surface fracture were visible on the corner of indentation. FIB result revealed the crack is likely extended long under surface.

3.2 Gold film – substrate system testing

The approach in this work was to deposit a metallic film on the ceramic to generate a film/substrate composite. A notable feature of film-substrate system indentation is, when the film is more compliant compare to the substrate, the stress concentration in the substrate is almost eliminated [14], suggesting a far less probability of fracturing in the substrate.

The hypothesis here is to assess the ceramic's influence on an indent that only penetrates the film portion of the composite; thereby, reducing the chance of forming defects in the ceramic. The Zhou-Prorok model was chosen as an analysis technique to decouple the film and substrate components of the indent [25, 26]. Gold was chosen as film material given its high ductility, inertness under ambient environment, and overall ease of deposition [34].

Figure 3.3 shows the extracted elastic modulus as a function of indent depth for a 475 nm thick gold film on the Al2O3 substrate. The modulus begins at approximately 100 GPa and increases continuously as the substrate is progressively engaged with penetration into the composite.

Direct parameter fitting was performed on this test result. Several combinations of parameters were chosen to find the best fit. The solid line is the result of the Zhou-Prorok model using fitted values of $E_f = 79\,GPa$, $\nu_f = 0.42$, $E_s = 475$ and $\nu_s = 0.226$. These values, with the exception of Es, are similar to literature values for gold and (0001) Al2O3 [32]. When the indenter reaches the film/substrate interface, dashed vertical line, the experimental data falls below the model and may indicate that cracks and defects are forming in the substrate. The agreement with the model when the indenter is within the

film is a good indication that the ceramic substrate is free of indentation generated defects. The Zhou-Prorok model is capable of detecting the substrate modulus.

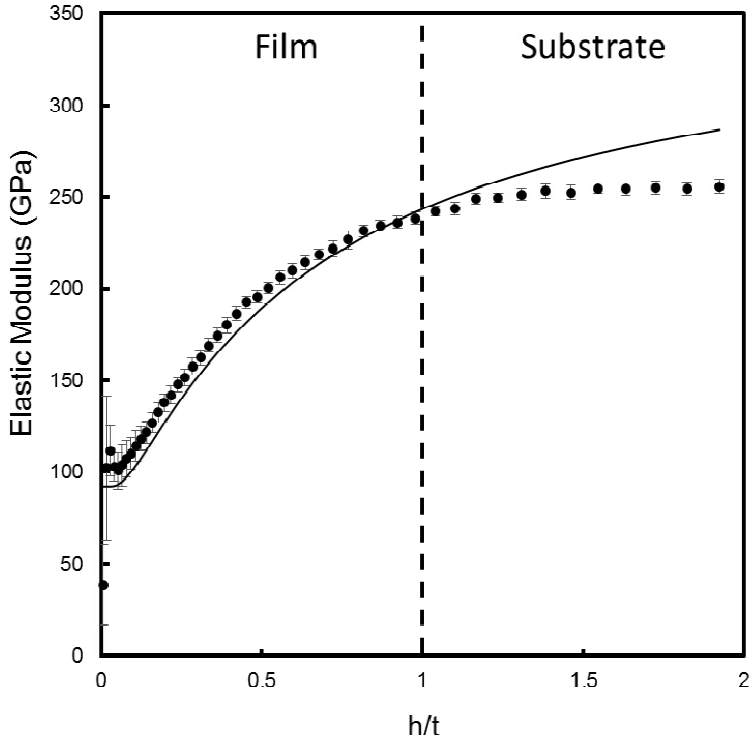

Figure 3.3. Indentation result on the gold film on Al2O3 single crystal (0001) substrate, the fitted Zhou-Prorok model shows good agreement if the indenter displacement is smaller than film thickness.

3.3 Conclusion on parameter fitting

The Zhou-Prorok model fits the data well enough (solid line in Figure 3.3); however, it relies upon estimating the ceramic's elastic modulus to fit the model to the experimental data. It also depends upon depositing a gold film of well-known film thickness and material properties. Given the number of parameters and variables, this can be a difficult task in laboratories with little film deposition experience. A more general method that does not rely upon knowledge of the film or even the substrate would better serve the indentation community.

Chapter 4 : Indirect method on testing brittle materials

4.1 Hyperbolic method development

Given the number of parameters and variables, this can be a difficult task in laboratories with little film deposition experience. A more general method that does not rely upon knowledge of the film or even the substrate would better serve the indentation community. The best way to accomplish this is to rearrange the Zhou-Prorok model to express it in terms of the substrate so as to mathematically separate the film and substrate components. In order to do so it is convenient to simplify some terms, namely;

$$h' = \frac{h}{t}\ and, \frac{1}{E_f'} = \frac{1}{E_f}\left(\frac{E_f'}{E_s'}\right)^{0.1}, \tag{4.1}$$

where h' is termed the reduced displacement. The Zhou-Prorok model can then be written as;

$$\frac{1}{E_t} = \frac{1}{E_f'}\left(1 - \mathrm{e}^{-\nu_s/h'}\right) + \frac{1}{E_s}\mathrm{e}^{-\nu_f/h'}, \tag{4.2}$$

The function of this form resembles a hyperbolic function. Hyperbolic csch functions are composed of a term of an exponential function and a term of one minus an exponential function. Noticeably, $\mathrm{csch}(1/x)$ has a property: it has an asymptote line and it approaches it very rapidly. This function and its asymptote are (Figure 4.1):

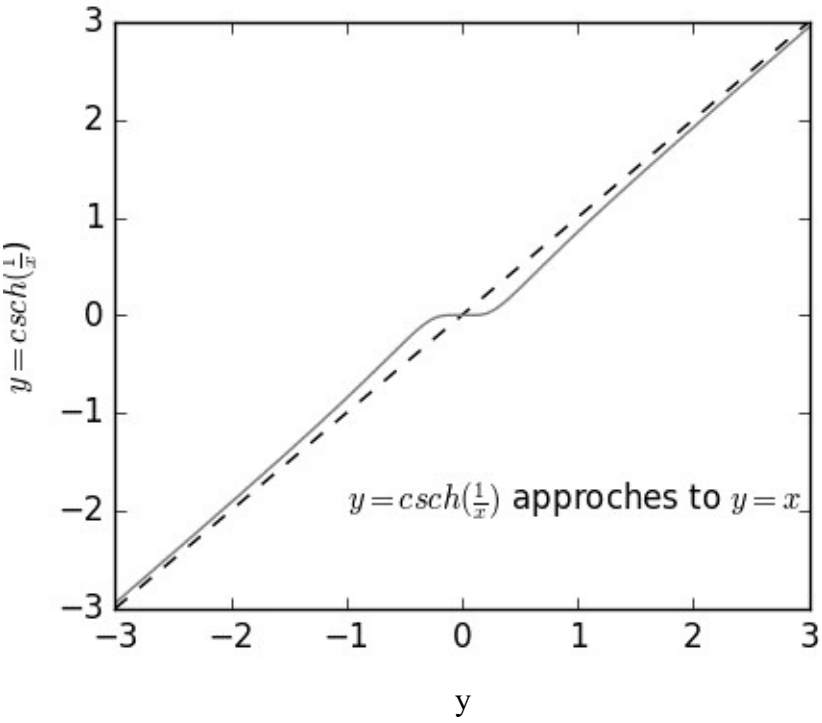

Figure 4.1 Hyperbolic function csch(1/x) (solid line) and its asymptote(dashed line).

$$\mathrm{y} = \ \mathrm{csch}(1/x) = \frac{2e^{-1/x}}{1 - e^{-2/x}} \tag{4.3}$$

$$y = x \tag{4.4}$$

It will be helpful to rearrange Zhou-Prorok model into a similar form. It is interesting to note that the substrate weighting factor on the film side has the form ($1 - exp(-1/x)$), which is a type of hyperbolic function [35];

(4.5)

$$F(x) = \frac{1}{2}\left(1 - \coth\left(-\frac{1}{2x}\right)\right) = \frac{1}{1 - e^{-\frac{1}{x}}}.$$

This function has a convenient property in that can be easily approximated by a linear function of the form $f(x) = 0.5 + x$, its asymptote [35]. By diving both sides of Equation (4.2) by the film side weighting factor we can obtain a similar form as in Equation (4.3);

$$\frac{1}{E_t}\ \frac{1}{\left(1 - e^{-\nu_s/h'}\right)} = \frac{1}{E'_f} + \frac{1}{E_s}\frac{e^{-\nu_f/h'}}{\left(1 - e^{-\nu_s/h'}\right)}. \tag{4.6}$$

Here, both sides of the equation have the form of Equation (4.5) with the potential to be linearly approximated by f(x) $= 0.5 + x$. The left side of the equation, referred to as $L(h')$ for convienance, contains the experimentally determined modulus and the substrate weighting factor ($1 - \exp(-\nu_s/h')$). Thus the data in Figure 3.4, which is the reciprocal of this equation, can be converted to this form by multiplying the measured modulus values by the substrate weighting factor with an estimation of the substrate Poisson's ratio.

In order to accomplish a linear approximation, it is necessary to apply hyperbolic identities to the left side of the equation, $\exp\left(-\nu_f/h'\right)/(1 - \exp(-\nu_s/h'))$, referred to as $I(h')$ for convenience; This treatment is detailed in the Appendix and result in an asymptote approximated by (figure 4.2);

$$I'(h') = 0.5 - \frac{\nu_f}{\nu_s} + \frac{h'}{\nu_s}. \tag{4.7}$$

Substituting this back into Equation (4.6) yields;

$$L(h') \approx \frac{1}{E'_f} + \frac{1}{E_s}\left(0.5 - \frac{\nu_f}{\nu_s} + \frac{h'}{\nu_s}\right), \tag{4.8}$$

This function is a linear function as the function has only one term related to the variable and it's a linear term. The slope of this function is $1/(E_s\nu_s)$. Because Zhou-Prorok model is a direct description to the experimental result. This treatment can be used on any experimental result. Thus, this offers a way to transfer experimental data into a linear function that can directly link to material property.

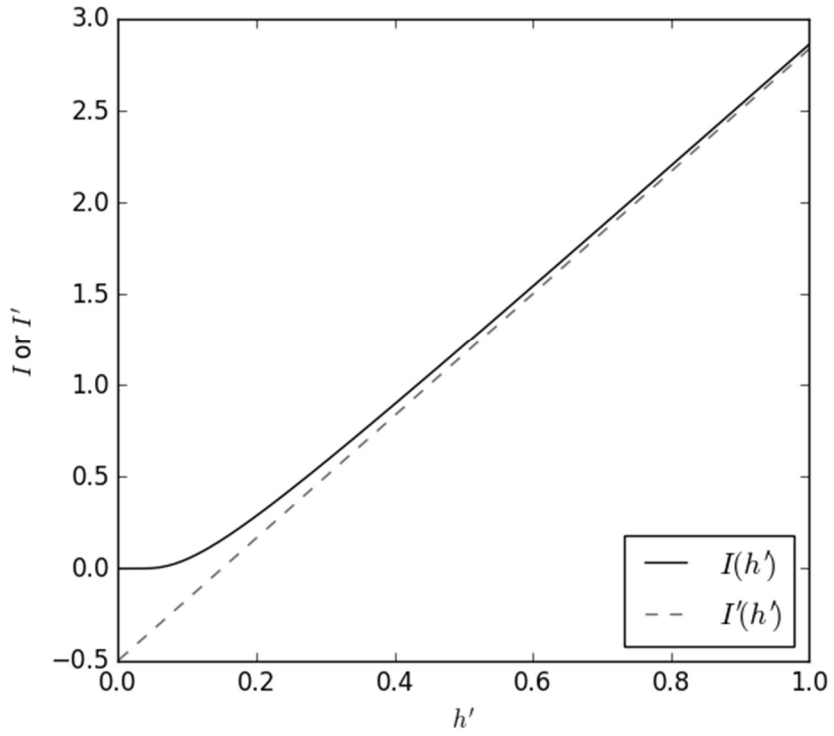

Figure 4.2 Function I and it's asymptote I' when ν_f and ν_s is 0.3. Two functions are very close at h' lager than 0.5.

4.2 Testing on Au film

To test the effectiveness of this method, the data from the previous experiment is used to generate L function. The value $(1 - \exp(-v_s/h'))$ is divided to each data point of the result and a line of data appears as a hyperbolic function. From the plot (Figure 4.3), the data appears as two parts: one part is curved, and the part where h' larger than around 0.7, is linear.

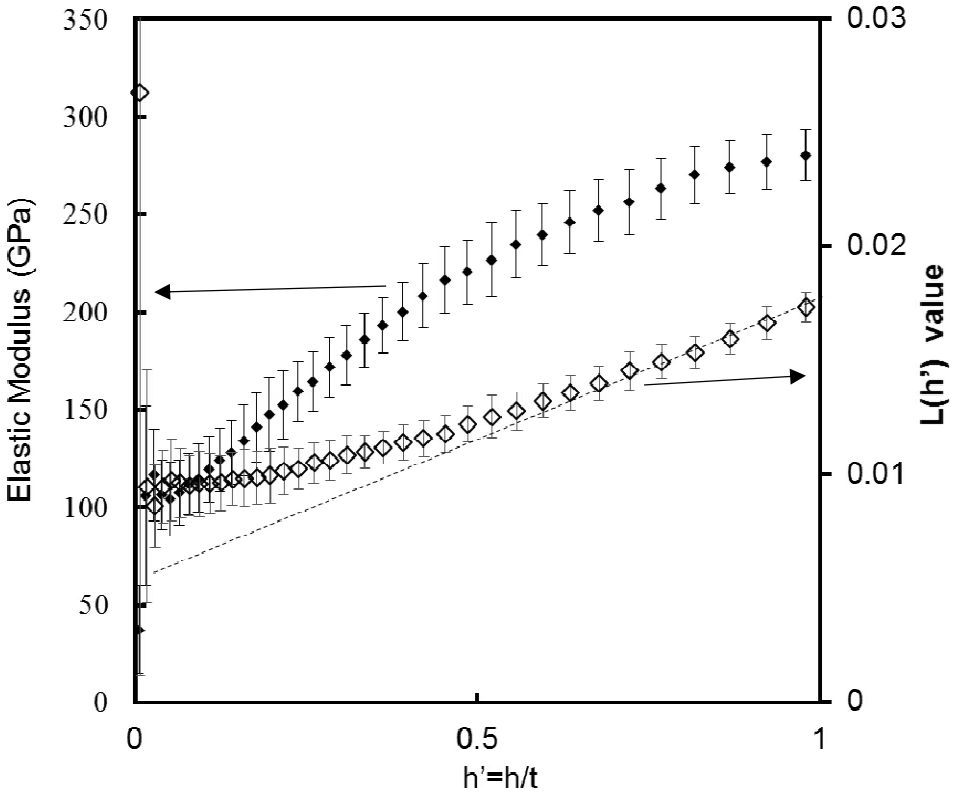

Figure 4.3 Indentation result on the gold film on Al2O3 single crystal (0001) substrate compare to the L function generated according to this result. L function shows a good linear behavior after h/t lager than 0.7.

This result shows previous analysis is valid when preforming on the real data from an indentation instrument. This is not surprising as the Zhou-Prorok model can successfully describe many film-substrate systems. The method mentioned in the previous section derived added no other assumption to this model, but only rearranged its terms.

Measuring the slope of the dashed line in Figure 4.3 reveals a value of 0.009576(1/GPa). Assuming $\nu_s = 0.226$, an elastic modulus of 427GPa is found for the substrate and comparable to literature values [32]. It should be noted that the literature substrate Poisson's ratio had to be assumed to perform this modulus determination. However, as the assumed Poisson's ratio became a component of the slope in treating the experimental data, it was essentially cancelled out when E_s was calculated. Had ν_s been assumed to be 0.300, the calculated modulus was still 446GPa. Thus, as long as ν_s values are assumed in the range of typical ceramics, there are only negligible effects on modulus determination.

4.3 Poisson's ratio's influence on this method

The above method introduced two functions associated with the reduced film thickness: $I(h')$, and its linear approximation $I'(h')$. The latter, was the asymptote line of the former. The accuracy of this method can be improved if $I(h')$ approaches $I'(h')$ much earlier in the indentation test.

These functions have one parameter that can be adjusted to achieve the most rapid approach: Poisson's ratio of the film. This can be controlled by selecting the film being deposited. Poisson's ratios are limited in range and enable a parameter space be developed to investigate how they impact the method. Thus, the film Poisson's ratio was varied between 0.1 to 0.4 and the substrate between 0.2 and 0.4.

Figure 4.5 plots values of $I(h')$, solid lines, and its linear asymptote $I'(h')$, dashed lines. In choosing any of the substrate Poisson's ratio plots, it was clear that the film Poisson's ratio had a major influence on how rapidly the two functions approached one another. Specifically, the lower the film Poisson's ratio, the faster they met. Although a film Poisson's ratio of 0.1 yielded the best results, it was not a practical choice as there are very few materials with a value this low. A survey of material candidates identified chromium as an ideal choice for the film. It is ductile, has a Poisson's ratio of 0.21 [27], is easily deposited via sputter deposition [34], and can wet most ceramics and form a strong interface [28].

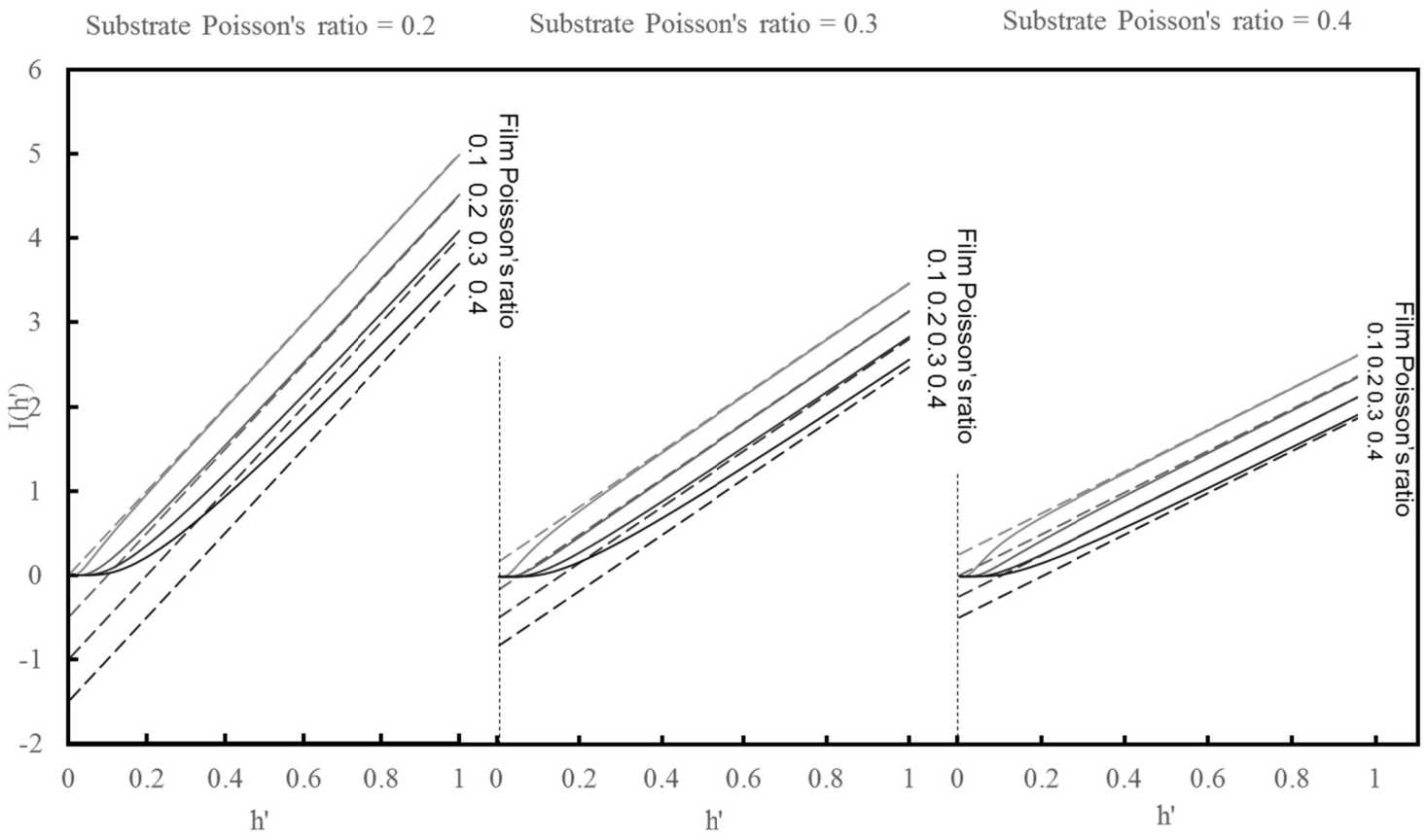

Figure 4.4 Behavior of I function and I' function under different Poisson's ratio combination of film and substrate. I' function approaches I function at different speed under different Poisson's ratio.

When the film Poisson ratio is minimized, the value of the substrate Poisson ratio is negligible in when the two functions approach each other, see Figure 4.5. This comparison also provides guidance in determining the range of data to select when determining slope. In the case of a chromium film in Figure 4.5, a *h'* range from 0.5 to 1.0 is suggested, which will be experimentally verified.

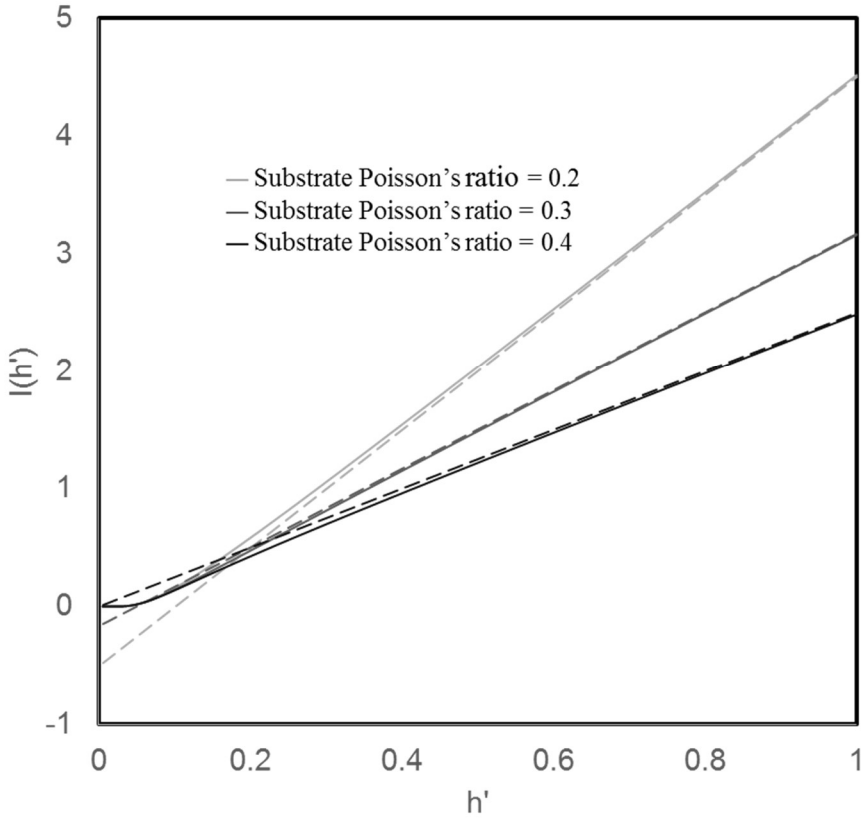

Figure 4.5 Behavior of I function and I' function provided that the film is Chromium with a Poisson's ratio of 0.21

4.4 Testing and result on Chromium Film

To demonstrate the advantage of using chromium over gold, indentation testing was performed on the aluminum oxide substrate after depositing a chromium film 380 nm thick. A plot of the measured elastic modulus versus displacement into the surface for the composite is shown in Figure 4.6, closed symbols. The modulus begins at a value near the film and increases to a value near the substrate, this kind of behavior indicates it is fitted to use the Zhou-Prorok mode to describe the result.

Similar data fitting process was done on this test result. A set of values were chased as the best fit (Table 4.1). With the gold data in Figure 4.4, the Zhou-Prorok model, solid line, fits the data well and suggests values for the material parameters involved, see Table 4.1.

Values of $L(h')$ and its linear approximation were determined in the same manner as in Figure 4.3. In comparing Figures 4.3 and 4.6, the chromium film data appeared to approach the asymptote line more rapidly than the gold film data. Thus, in principle, the slope can

be extracted from more data points and yield a more accurate value. This yielded a substrate modulus of 458GPa, which is a reasonable value considering the 396GPa modulus measured in the presence of fractures during direct indentation.

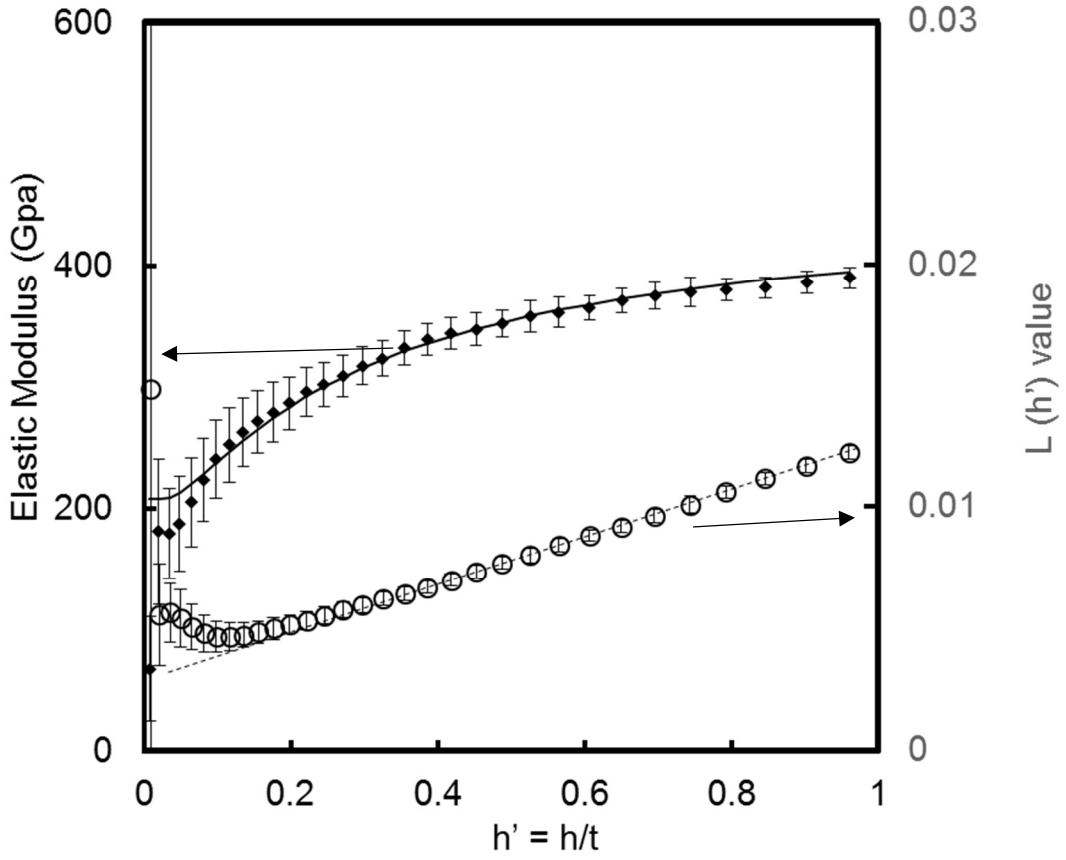

Figure 4.6 Indentation result on the Chromium film on Al2O3 single crystal (0001) substrate compare to the L function generated according to this result. L function shows a good linear behavior after h/t lager than 0.5.

Table 4.1 The thickness of deposited film and parameter fitting result

Film/Substrate	Thickness	Film Poisson's value	Substrate Poisson's value	Fitted Elastic modulus Film(GPa)	Fitted Elastic modulus Substrate(GPa)
Au/Al2O3	475nm	0.420	0.226	79	480
Cr/Al2O3	380nm	0.210	0.226	190	460
Cr/MgO	380nm	0.210	0.239	250	360
Cr/SiC	380nm	0.210	0.175	210	510
Cr/CaCO3	380nm	0.210	0.310	280	80
Cr/Fused Silica	380nm	0.210	0.180	280	80

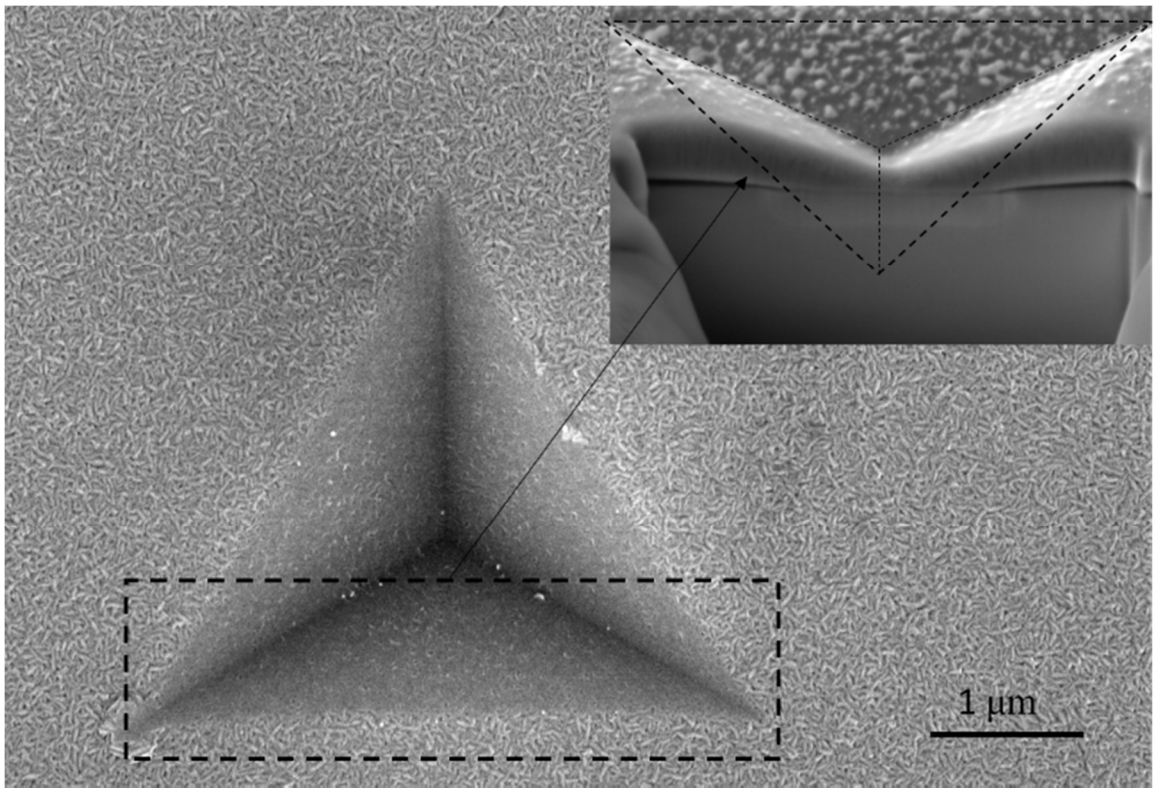

Figure 4.7. Scanning electron microscope of residual indentation on the Al2O3 single crystal (0001) with a Chromium film. Surface fracture cannot be observed. FIB result revealed there is no sign of crack.

In comparing the indentation behavior directly on the ceramic to the film on ceramic, the experimental results from the film-substrate system were significantly more predictable. It behaved almost as closely as the Zhou-Prorok model described as long as the indenter did not penetrate into the substrate. The presence of the film avoided the generation of stress singularities that could potentially result in crack nucleation and growth. In fact, a focused-ion-beam cross-section of an indent in the film-substrate system did not reveal any fractures in the aluminum oxide substrate, see Figure 4.7. Underneath the chromium film, there was

only a step which was caused by the different sputtering rate of the aluminum oxide and the chromium. And inside the aluminum substrate, there was no apparent fracture could be observed.

4.5 Testing on Other Substrate

To demonstrate that the chromium film method was applicable to a variety of ceramic materials, it was performed on SiC, MgO, fused silica and CaCO3 ceramic substrates. Elastic properties of those materials are in Table 4.2. Figure 4.8 (a) shows a compilation of measured elastic modulus as a function of indent depth. In all cases, the data generally begin at a value near the film elastic modulus and either increased to or decreased to a value near the substrate elastic modulus, as Zhou-Prorok model predicted.

It is interesting to note that the MgO data exhibit a tailing off of the data when the indenter has penetrated approximately 80% of the film thickness. This is an indication that the MgO substrate is likely fracturing at this penetration depth. The harmonic displacement of this particular testing cannot sustain enough value after 80% of the film thickness, this can be attributed to the high stiffness and low hardness of this composite, and can cause experimental error (figure 4.9). There is a clear step around 80% of film thickness in the raw data from the instrument. As this is formed by the limitation of the instrument itself, there was no good solution to correct those data. Therefore, it is prudent to exclude the data past this point for MgO.

The indentation data in figure 4.8 (a) was then converted to $L(h')$, as above, and plotted in figure 4.8 (b). Using the h' range from 0.5 to 1.0, the slopes of each was determined and a substrate modulus calculated, see Table 2. In nearly all cases, the indirect modulus was greater than the direct modulus and matched rather well with values found in the

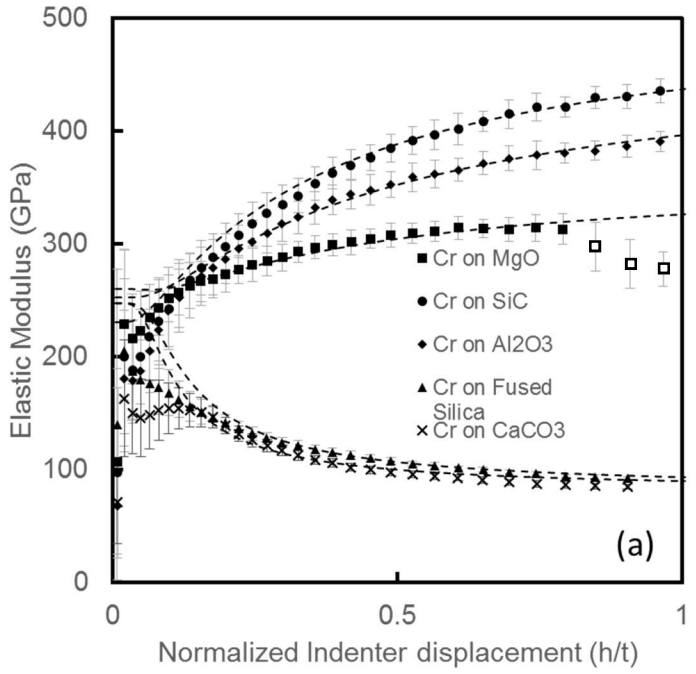

(a)

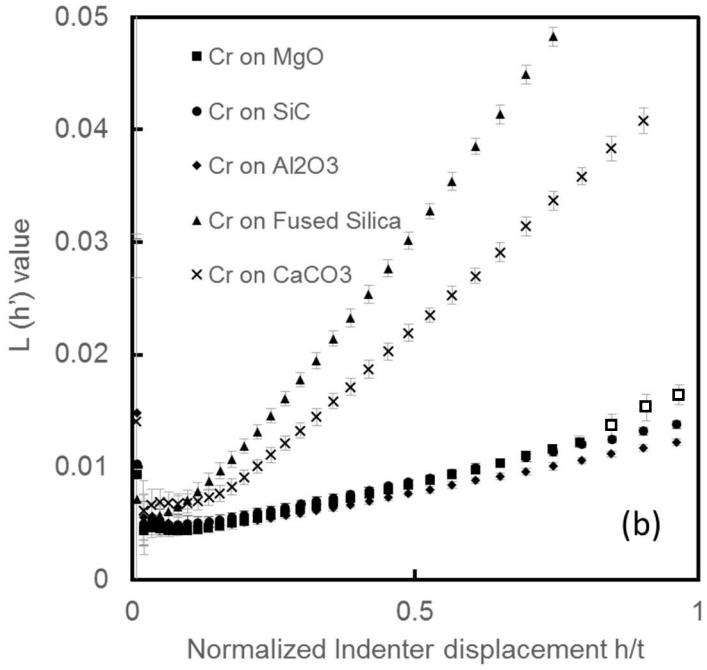

(b)

Figure 4.8 Indentation result on the Chromium film on single crystal substrate (a) compare to the L function generated according to those test result (b).

Table 4.2 Test result

Material	Elastic modulus (literature value)		Poisson's ratio		Direct Indentation (GPa)	Indirect Indentation (GPa)
Al_2O_3 (0001)	553.5([0001])	[29,32]	0.226	[32]	396(±9)	458(±10.5)
MgO (100)	330	[30]	0.239	[30]	290(±5)	330(±10)
SiC – 6H (0001)	516.5([0001])	[29,32]	0.175	[32]	495.5(±10)	522(±11)
$CaCO_3$(100)/<001>	69.9	[33]	0.31	[33]	73.6(±3)	70(±3)
Fused Silica	72	[6]	0.18	[6]	69.5(±5)	76(±2.0)

* single crystal, parentheses shows its orientation
[ ] literature references

literature. The CaCO3 substrate possessed a slightly larger direct modulus deemed to be within the experimental error and the Al2O3 indirect modulus was somewhat below its literature value. Given that it has a highly anisotropic rhombohedral crystal structure, indentation is expected to engage a complex mixture of directional deformations.

In this method, a h' range from 0.5 to 1.0 was employed to determine the slope of the $L(h')$ asymptote. To confirm that this was a reasonable range to use, the instantaneous slope of the $L(h')$ curve was calculated to determine its consistency in this range, see Figure 4.10.

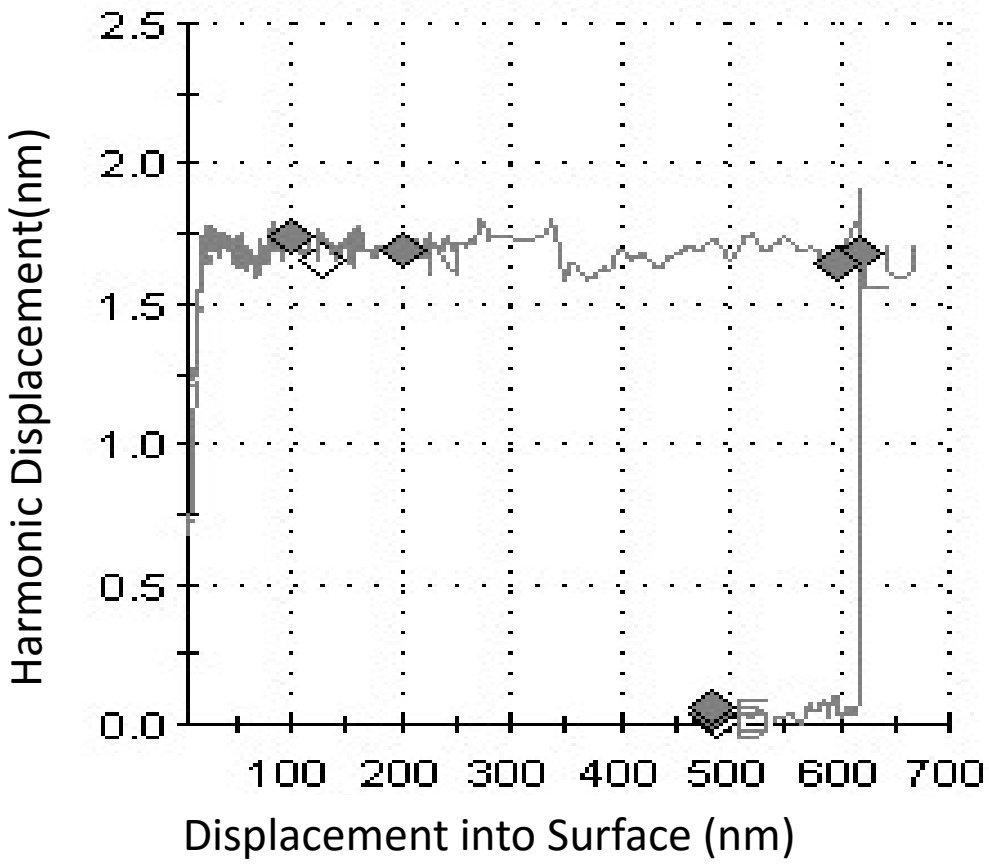

Figure 4.9 Raw data from indenter shown the Harmonic displacement inconsistent

Here, it was clear that the slope was consistent in the *h'* range from 0.5 to 1.0. For low modulus materials this range is significantly wider beginning at *h'* of approximately 0.2.

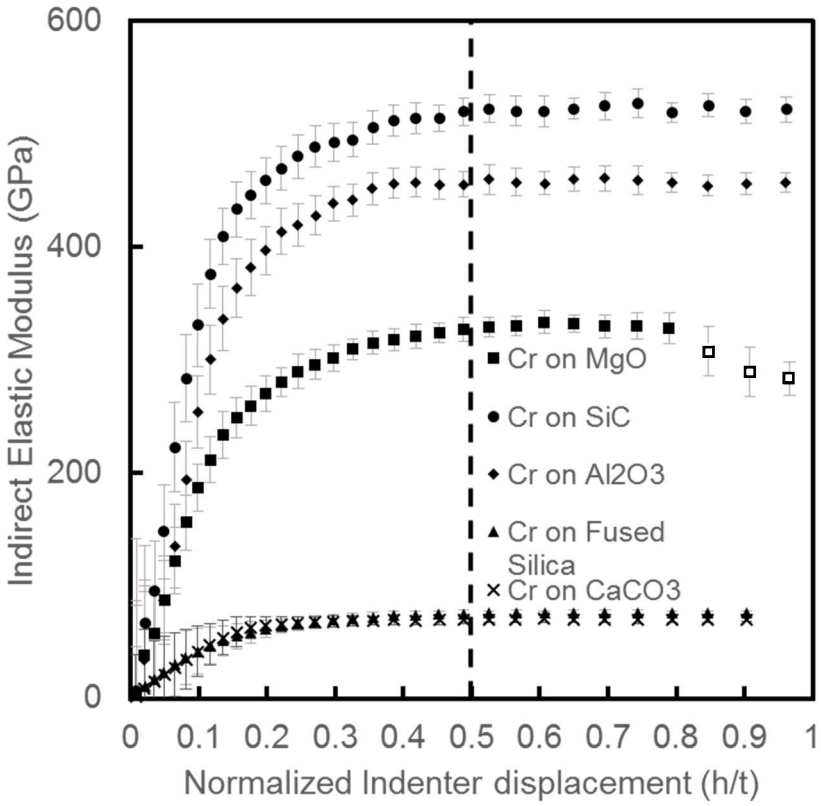

Figure 4.10 Extracted indirect indentation result generated from figure.4.4 (b). Point after 0.5 of normalized displacement were indirect indentation result modulus.

The agreement of indirect moduli results in Table 2 to literature values demonstrated that the elastic modulus of brittle materials can be ascertained by employing a deposited film to eliminate fracture when directly indented. This method decoupled the substrate's contribution to the composite and measured it directly. A very useful feature is that this did not require any assumptions about the material properties involved, meaning it can be applied to any unknown film-substrate composite as long as the film thickness is roughly known. Preferably, depositing a well-known film material with low Poisson's ratio facilitates an easier and more accurate determination of the substrate's properties. Chromium metal was found to be the ideal practical choice.

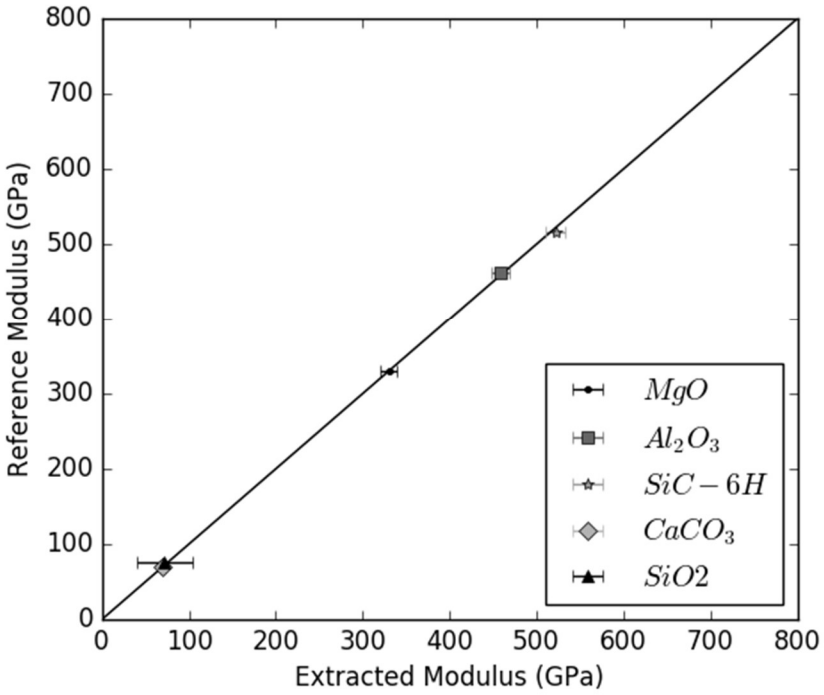

Figure 4.11 Elastic modulus value from literature vs. Elastic modulus value from this work, shows good agreement with each other.

Chapter 5 : Conclusions

This work presented a new method to test the nanoindentation elastic modulus of brittle materials. Compared to direct indentation, it gives a far more accurate and reliable value. By applying a medium film, this method can give a more reliable result than direct indentation for brittle materials. This method is developed on the Zhou-Prorok model. In conclusion:

- Zhou-Prorok model can be rearranged as a hyperbolic function.
- This hyperbolic function has a distinct asymptote that directly relates to the Poisson's value and elastic modulus of the substrate.
- Applying this method to a film-substrate system can decouple the substrate modulus from the composite modulus tested from the indentation instrument.
- For several brittle materials, chromium film works well because of its low Poisson's ratio and can wet the ceramic surface.
- For an unknown film-substrate system, with only the film thickness known, this method can give a good estimation of both film and substrate nanoindentation elastic modulus.

Appendix

The famous Euler's formula shows the relationship between triangular function and exponential functions with an imaginary variable. Similarly, there is another set of formulas that describes the relationship between exponential functions with real numbers as variables and other kinds of functions. These types of functions are called hyperbolic functions. They are of great importance in many fields, including in approximate the exponential function [35].

It is well known that:

$$\tan x \approx x,$$

when x is small. And similarly we have such relations:

$$\tanh(x) \approx x,$$

Employing the hyperbolic function identity [35], we can transform the $I(h')$ function to the form of a hyperbolic function:

$$I(h') = \frac{1}{2}\exp\left(-\frac{\nu_f}{h'}\right)\left(1 - \coth\left(-\frac{\nu_s}{2h'}\right)\right)$$

Replace the exponential function with the hyperbolic function, we get:

$$I(h') = \frac{1}{2}\left(\exp\left(-\frac{\nu_f}{h'}\right) - \cosh\left(-\frac{\nu_f}{h'}\right)\left(\frac{\tanh\left(-\frac{\nu_f}{h'}\right)}{\tanh\left(-\frac{\nu_s}{2h'}\right)} - \frac{1}{\tanh\left(-\frac{\nu_s}{h'}\right)}\right)\right);$$

The asymptote can be calculated by simply replacing $\exp(-1/x)$ and $\cosh(1/x)$ with 1, and $\tanh(a/x)$ with a. The asymptote line of the function $I(h')$ can be written as:

$$I'(h') = 0.5 - \frac{\nu_f}{\nu_s} + \frac{h'}{\nu_s}$$

REFERENCES

[1] M. F. Doerner and W. D. Nix: A method for interpreting the data from depth-sensing indentation instruments. *J. Mater. Res.* **1**, 601, (1986).

[2] K.E. Petersen, , C.R. Guarnieri: Young's modulus measurements of thin films using micromechanics. *J. Applied Phy.* **50**, 6761–6766, (1979).

[3] R. B. King: Elastic Analysis of Some Punch Problems for a Layered Medium. *Int. J. Solids Struct.,* **23**, 1657, (1987).

[4] K.W. McElhaney, J.J. Vlassak, W.D. Nix: Determination of indenter tip geometry and indentation contact area for depth-sensing indentation experiments. *J. Mater. Res.* **13**, 1300–1306, (1998)

[5] W. C. Oliver and G. M. Pharr: An improved technique for determining hardness and elastic modulus using load and displacement sensing indentation experiments. *J. Mater. Res.* **7**, 1564, (1992).

[6] G. m. Pharr, W.C. Oliver, F.R. Brotzen: On the generality of the relationship among contact stiffness, contact area, and elastic modulus during indentation. *J. Mater. Res.* **7**, 613–617, (1992). doi:10.1557/JMR.1992.0613

[7] W. C. Oliver and G. M. Pharr: Measurement of hardness and elastic modulus by instrumented indentation: Advances in understanding and refinements to methodology. *J. Mater. Res.* **19**, 3 (2004).

[8] X. Li and B. Bhushan: A review of nanoindentation continuous stiffness measurement technique and its applications. *Materials Characterization,* **48**, 11, (2002).

[9] G.M. Pharr, A. Bolshakov: Understanding nanoindentation unloading curves. *J. Mater. Res.* **17**, 2660–2671, (2002).

[10] G. M. Pharr: Measurement of mechanical properties by ultra-low load indentation. *Materials Science and Engineering: A,* **253**, 151, (1998).

[11] D.S. Harding, W.C. Oliver, G.M. Pharr:Cracking During Nanoindentation and its Use in the Measurement of Fracture Toughness, in: *Symposium B2 – Thin Films: Stresses and Mechanical Properties* **V** (1994)*MRS Online Proceedings Library*.

[12] R.F. Cook, G.M. Pharr, . Direct observation and analysis of indentation cracking in glasses and ceramics. *J. Am. Ceram. Soc:***73**, 787–817(1990).

[13] I.N. Sneddon: The relation between load and penetration in the axisymmetric boussinesq problem for a punch of arbitrary profile. *Int. J. Eng. Sci.* **3**, 47–57(1965)

[14] J. Li, T.-W. Chou,. Elastic field of a thin-film/substrate system under an axisymmetric loading. *Int. J. Solids Struct.* **34**, 4463–4478, (1997) doi:10.1016/S0020-7683(97)00053-X

[15] H. Gao, C.-H. Chiu, and J. Lee: Elastic contact versus indentation modeling of multi-layered materials. *Int. J. Solids Struct.,* **29**,2471, (1992).

[16] T.Y. Tsui, G.M. Pharr: Substrate effects on nanoindentation mechanical property measurement of soft films on hard substrates. *J. Mater. Res.* **14**, 292–301(1999).

[17] R. Saha, W.D. Nix: Effects of the substrate on the determination of thin film mechanical properties by nanoindentation. *Acta Materialia* **50**, 23–38,(2002)

[18] J. Menčík, D. Munz, E. Quandt, E.R. Weppelmann, M.V. Swain:. Determination of elastic modulus of thin layers using nanoindentation. *J. Mater. Res.* **12**, 2475–2484,(1997).

[19] D.S.Stone,. ELASTIC REBOUND BETWEEN AN INDENTER AND A LAYERED SPECIMEN : PART I. MODEL. *J. Mater. Res.* **13**, 3207–3213,(1998).

[20] K.B. Yoder, D.S. Stone, R.A. Hoffman, J.C. Lin: Elastic rebound between an indenter and a layered specimen: Part II. Using contact stiffness to help ensure reliability of nanoindentation measurements. *J. Mater. Res.* **13**, 3214–3220,(1998).

[21] N. Schwarzer: Arbitrary Load Distribution on a Layered Half Space. *J. Tribol* **122**, 672–681,(2000).

[22] T. Chudoba, N. Schwarzer, F. Richter,. Determination of elastic properties of thin films by indentation measurements with a spherical indenter. *Surf. Coat. Technol.* **127**, 9–17,(2000).

[23] Y,-G. Jung, B.R. Lawn, M. Martyniuk, H. Huang, X.Z. Hu: Evaluation of elastic modulus and hardness of thin films by nanoindentation. *J. Mater. Res.* **19**, 3076–3080,(2004).

[24] A. Perriot, E. Barthel, Elastic contact to a coated half-space: Effective elastic modulus and real penetration. *J. Mater. Res.* 19, 600–608,(2004).

[25] B. Zhou and B. Prorok: A Discontinuous Elastic Interface Transfer Model of Thin Film Nanoindentation. *Experimental Mechanics,* **50**,793, (2010).

[26] B. Zhou and B. C. Prorok: A new paradigm in thin film nanoindentation, *J. Mater. Res.* vol. 25, pp. 1671-1678, (2010).

[27] G.V. Samsonov, M.E. Straumanis: Handbook of the Physicochemical Properties of the Elements. *Physics Today* **21**, 97–97(2009).

[28] M.Ohring, Materials science of thin films. *Academic press*, (2001).

[29] J.F. Shackelford, W. Alexander: CRC materials science and engineering handbook. CRC, Boca Ratan(2001)

[30] D.-H. Chung, Elastic moduli of single crystal and polycrystalline MgO. *Philosophical Magazine* **8**, 833–841(1963).

[31] J.J. Wortman, R.A. Evans: Young's Modulus, Shear Modulus, and Poisson's Ratio in Silicon and Germanium. *J. Appl. Phys.* **36**, 153–156,(1965).

[32] R. Thokala, J. Chaudhuri: Calculated elastic constants of wide band gap semiconductor thin films with a hexagonal crystal structure for stress problems. *Thin Solid Films* **266**, 189–191,(1995).

[33] C.-C. Chen, C.-C. Lin, L.-G. Liu, S.V. Sinogeikin, J.D. Bass: Elasticity of single-crystal calcite and rhodochrosite by Brillouin spectroscopy. *Am. Mineral* **86**, 1525–1529,(2001).

[34] M. Sullivan, B.C. Prorok, B.C: Evaluating indent pile-up with metallic films on ceramic-like substrates. *J. Mater. Res.* 30, 2046–2054,(2015).

[35] M. Hazewinkel: Hyperbolic functions, *Encyclopedia of Mathematics,* Springer(2001), ISBN 978-1-55608-010-4

[36] Goldstein, Herbert. Classical mechanics. Pearson Education India, 1965.